EFDA–JET–PR(09)10

M. Gatu Johnson, C. Hellesen, E. Andersson Sundén, M. Cecconello, S. Conroy, G. Ericsson, G. Gorini, V. Kiptily, M. Nocente, S. Pinches, E. Ronchi, S. Sharapov, H. Sjöstrand, M. Tardocchi, M. Weiszflog and JET EFDA contributors

Neutron Emission from Beryllium Reactions in JET Deuterium Plasmas with ^{3}He minority

Neutron Emission from Beryllium Reactions in JET Deuterium Plasmas with ^{3}He minority

M. Gatu Johnson[1], C. Hellesen[1], E. Andersson Sundén[1], M. Cecconello[1], S. Conroy[1], G. Ericsson[1], G. Gorini[2], V. Kiptily[3], M. Nocente[2], S. Pinches[3], E. Ronchi[1], S. Sharapov[3], H. Sjöstrand[1], M. Tardocchi[2], M. Weiszflog[1] and JET EFDA contributors*

JET-EFDA, Culham Science Centre, OX14 3DB, Abingdon, UK

[1]Department of Physics and Astronomy, Uppsala University, Box 516, SE-75120 Uppsala, Sweden EURATOMVRAssociation
[2]Physics Department, Milano-Bicocca University, and Istituto di Fisica del Plasma del CNR, Milan, Italy EURATOM-ENEA-CNR Association
[3]EURATOM-UKAEA Fusion Association, Culham Science Centre, OX14 3DB, Abingdon, OXON, UK
** See annex of F. Romanelli et al, "Overview of JET Results",*
(Proc. 22 [nd] IAEA Fusion Energy Conference, Geneva, Switzerland (2008)).

Preprint of Paper to be submitted for publication in
Nuclear Fusion

ABSTRACT.

Recent fast ion studies at JET involve ICRF heating tuned to minority ^{3}He in cold deuterium plasmas, with beryllium evaporation in the vessel prior to the session. During the experiments, the high-resolution neutron spectrometer TOFOR was used to study the energy spectrum of emitted neutrons. Neutrons of energies up to 10MeV, not consistent with the neutron energy spectrum expected from d(d,n)^{3}He reactions, were observed. In this paper, we interpret these neutrons as a first-time observation of a ^{9}Be(^{3}He,n)^{11}C neutron spectrum in a tokamak plasma, a conclusion based on a consistent analysis of experimental data and Monte Carlo simulations. ^{9}Be(α,n)^{12}C and ^{9}Be(p,n)^{9}B reactions are also simulated for p and α fusion products from d(^{3}He,α)p reactions; these two-step processes are seen to contribute on a level of a few percent of the single-step process in ^{9}Be(^{3}He,n)^{11}C. Contributions to the total neutron yield from the ^{9}Be(^{3}He,n)^{11}C reaction are found to be in the range18-64%. We demonstrate how TOFOR can be used to simultaneously i) probe the deuterium distribution, providing reliable measurements of the bulk deuterium temperature, and ii) provide an independent estimate of the beryllium concentration. The observation of ^{9}Be related neutrons is relevant in view of the upcoming installation of a beryllium-coated ITER like wall on JET, and for ITER itself. An important implication is possible neutron-induced activation of the ITER vessel during the low activation phase with ICRF heating tuned to minority ^{3}He in hydrogen plasmas.

1. INTRODUCTION

One of the envisaged heating schemes for ITER is ICRF tuned to the second harmonic resonance of tritium, with co-resonant fundamental absorption on minority ^{3}He [1]. This heating scheme has been shown not to suffer from parasitic absorption on alpha particles or beryllium [2]. Beryllium will be one of the main materials used in the ITER first wall. In preparation for ITER steady state scenarios, it is planned to install an ITER-like wall with beryllium coatings at JET. This will cause an increase in beryllium concentration in the plasma core compared to today. Experiments in which JET deuterium plasmas were heated by Ion Cyclotron Radio Frequency (ICRF) heating tuned to the fundamental resonance frequency of ^{3}He following beryllium evaporation have been carried out. The subject of study during these JET experiments was the dynamics of fast ions, their redistribution and losses and their correlation with Magneto Hydro Dynamic (MHD) activity in the plasma [3,4]. In this paper, we report on the observation during the experiments of a more complex neutron energy spectrum to which the neutrons produced in the ^{9}Be(^{3}He,n)^{11}C reaction contribute significantly.

Neutron emission spectroscopy is used as a fast fuel ion diagnostic for deuterium and deuterium-tritium tokamak plasmas. Information about the fast fuel ion distributions can be obtained through analysis of the measured neutron spectrum. The regular neutron emission from deuterium plasmas, from the reaction d(d,n)^{3}He, is a spectrum centered at 2.5MeV and broadened due to kinematic effects [5]. Neutral Beam (NB) heating with 130keV deuterium beams gives a broadening in the range 2-3MeV. In the present experiment, neutrons with energies up to ~10MeV were observed. Radio frequency heating tuned to deuterium could accelerate deuterium ions to sufficiently high

energies to produce neutrons with energies E_n>3 MeV, but no such heating was employed during these experiments.

Several reaction mechanisms have previously been invoked to explain high-energy neutrons or anomalous rates in the neutron emission. Below, we consider i) so-called knock-on reactions, ii) triton burn-up and iii) reactions between fuel ions and plasma impurities.

In knock-on processes, deuterium ions with high energy could be produced through elastic collision energy transfer from other fast particles present in the plasma. The imprint of this type of process in the neutron emission has been previously simulated [6] and observed [7] in the case of alpha particle knock-on in deuterium-tritium plasmas. Two different sources of fast ions that could participate in knock-on reactions can be identified: RF heated minority ions and fast fusion products. The two processes are similar but for the difference in source term distribution. Knock-on processes in ICRF heated deuterium plasmas with minority ^{3}He have been modelled in detail in [8]. To summarize, fusion reactions between fast deuterium from ICRF heated ^{3}He knock-on and bulk deuterium are expected to result in a distinguishable high energy knock-on tail in the neutron spectrum with amplitude up to several percent of the bulk neutron peak depending on coupled RF power and ^{3}He density. Fusion product knock-on in these plasmas, on the other hand, is found to be on a level $<10^{-4}$ of the bulk neutron peak amplitude. The intensity of the fast neutron distribution is found to fall off roughly exponentially with the slope correlated to the ^{3}He distribution function. Knock-on reactions contribute to the high-energy events observed here.

Neutrons from d(t,n)α reactions are produced also in deuterium plasmas due to the production of tritium in d(d,p)t reactions; this is the so called Triton BurN up (TBN) process. The effect has been extensively studied in e.g. [9] (and references therein) but will be shown not to explain the high energy neutrons observed in this case.

Neutrons from fusion reactions between ICRF heated light ions and impurity species present in the plasma can interfere with the measured d(d,n)^{3}He neutron spectrum, as established in [10], where the observation of ^{9}Be(p,n)^{9}B neutrons was claimed for plasmas with ICRF tuned to the fundamental hydrogen resonance. Such anomalous neutron production has also been discussed for tritium plasmas in [11], where t(p,n)^{3}He fusion reactions were established as the source of an observed 40% contribution to the measured neutron rate from non- d(t,n)α neutrons, using the fact that fast protons with energy well above the reaction threshold were observed by both gamma spectrometers and a Neutral Particle Analyzer (NPA) and consistent with PION modelling. In this latter case, the level of the anomalous contribution could be established using the fact that the t(p,n)^{3}He neutrons fall in a different energy range than d(t,n)α neutrons. The total measured rate could be compared with the measured 14MeV neutron rate to determine the t(p,n)^{3}He contribution.

We identify the ^{9}Be(^{3}He,n)^{11}C, ^{9}Be(α,n)^{12}C and ^{9}Be(p,n)^{9}B reactions (together with knock-on) as the most likely sources of the high energy neutrons observed in this experiment. The presence of ^{3}He in the MeV energy range is confirmed through gamma spectroscopy measurements. Fast alpha and protons will be present as fusion products from the d(^{3}He,p)α reaction. Simulations are used to

show that the largest contribution originates from $^{9}Be(^{3}He,n)^{11}C$. The main impurity in the JET vessel (in the case of no beryllium evaporation) is carbon. Reactions between fuel ions and carbon impurity have also been considered; these reactions could be disregarded due to their endothermic nature with corresponding high projectile energy thresholds, and low cross sections.

A contribution of about 10% to the neutron yield in deuterium-tritium plasmas from neutrons from the $^{9}Be(\alpha,n)^{12}C$ reaction was established indirectly in [12] through measurements of gamma from the excited carbon nucleus produced in the reaction. No $^{9}Be(^{3}He,n)^{11}C$ neutron spectrum measurements in tokamak plasmas have previously been reported, but the reaction was invoked as the source of an observed low neutron rate during a mode conversion hydrogen plasma experiment with minority ^{3}He heating at JET in [13]. This scenario is one of the foreseen modes of operation during the ITER low activation phase; a high level of $^{9}Be(^{3}He,n)^{11}C$, neutron production might affect the feasibility of the scheme for ITER.

A contribution to the $d(d,n)^{3}He$ neutron spectrum from the $^{9}Be(^{3}He,n)^{11}C$, $^{9}Be(\alpha,n)^{12}C$ and $^{9}Be(p,n)^{9}B$ reactions cannot be easily isolated since the energy ranges for neutrons emitted in the reactions overlap, as will be shown. A high-resolution neutron spectrometer is thus necessary for this task; here we use the TOFOR neutron spectrometer [14].

The paper is organized as follows. After a detailed description of the experiment scenario in section 2, we will present simulation results showing the expected shape of $^{9}Be(^{3}He,n)^{11}C$, $^{9}Be(\alpha,n)^{12}C$ and $^{9}Be(p,n)^{9}B$ neutron spectra as well as an assessment of the contribution from these reactions to the total neutron rate (section 3). Then, in section 4, results from neutron emission spectroscopy measurements will be presented and the experimental observation of $^{9}Be(^{3}He,n)^{11}C$ neutrons established. The measurements will be compared with the simulations, and we will show how the comparison yields an estimate of the beryllium concentration in the JET pulses studied.

2. EXPERIMENT

JET pulses from two experimental sessions with deuterium plasmas seeded with ^{3}He on a level of 1-7% were studied for this paper. The main heating for both sessions was ICRH tuned to the fundamental ^{3}He frequency. In the second session, also Lower Hybrid Current Drive (LHCD) heating was applied for the purpose of changing the q profile to provoke MHD activity. Diagnostic NB heating blips were applied at the beginning and end of each pulse, but in the data studied these were excluded to avoid contamination of beam-plasma neutron emission. A typical plasma scenario from the second session is illustrated in Figure 1, where the auxiliary heating power, the neutron yield, the electron density and the electron temperature are shown as functions of plasma time for JET Pulse No:73765.

Both experiments involved overnight beryllium evaporation to enhance the gamma emission from the plasma for diagnostic purposes, with two evaporation heads used before the first session and four before the second. Properties of the pulses studied are summarized in Table 1. As can be seen, different plasma currents were scanned. This resulted in different fast ion confinement. The

RF power also varied during the session resulting in varying levels and energies of produced fast ions. Finally, the ^{3}He concentration varied from 1-7 percent with an impact on RF coupling and fast ion production.

For the majority of the pulses, the RF resonance layer (R_ω) was at 2.86m ($\omega_{RF} = 37$MHz, $B_T = 3.45$T). Exceptions are Pulse No's: 73766, with $\omega_{RF} = 33$MHz and $B_T = 3.45$ T giving $R_\omega = 3.24$m, and 73213 and 73214, with $\omega_{RF} = 33$MHz, $B_T = 3.35$T and $R_\omega = 3.12$m.

The presence of fast ^{3}He ions is confirmed by gamma spectroscopy measurements. The effective ^{3}He temperature T ^{3}He is estimated from analysis of gamma spectroscopy data of the $^{12}C(^3He,p)^{14}N^*$, $^9Be(^3He,n)^{11}C^*$ and $^9Be(^3He,p)^{11}B^*$ reactions (Figure 2) using the method described in [19] to be 200-350keV.

During the experiments, the TOFOR neutron spectrometer [14] was used to measure the emitted neutron spectrum. TOFOR is a time-of-flight neutron spectrometer located in the JET roof laboratory with a vertical line-of-sight through the plasma core. It consists of two detector sets, the primary with 5 detectors in the collimated beam of neutrons incident from the plasma and the secondary with 32 detectors at a distance 1.2 m from the first. The time-of-flight (t_{TOF}) spectrum is constructed post discharge from time differences between events recorded in the two detector sets. Both true coincidences, i.e., events corresponding to a single neutron interacting in both the primary and the secondary detectors, and random events, i.e., uncorrelated detections that are not due to the same neutrons, will be constructed in this way. The random events will show up as a flat level, proportional to the total count rate in the primary and secondary detectors, across the entire spectrum. The level of random events is determined from data on the negative t_{TOF} side and used as input in the analysis when physical parameters are determined. For true events between the detector set center points, $t_{TOF} = 1.02 \cdot 10^{-7} E_n^{-1/2}$ ns, for E_n given in MeV. Thermonuclear neutron emission from $d(d,n)^3He$ fusion reactions with E_n around 2.5MeV will show up as a peak at 65ns on the t_{TOF} scale. TOFOR cannot generally claim observations at intensity below the percent level compared to the main $d(d,n)^3He$ peak due to the presence of random events in the spectrum.

In the analysis, we will need an estimate of the fraction of the total neutron emission in the TOFOR Line Of Sight (LOS). The vertical TOFOR LOS is centered at a major radius $R_{maj} = 2.88$m (Figure 3). The total number of neutrons emitted in the plasma volume viewed by TOFOR is obtained by dividing the measured flux, I_{LOS}, with the solid angle of the sight line, Ω_{LOS}. If the emitting plasma volume, V_{TOT}, is also known, this number can be turned into an emissivity by dividing with the size of the emitting volume viewed by TOFOR, V_{LOS}. The emitting volume was modelled as a torus of constant emissivity bounded by the minor radius r_{min} and with major radius fixed at the magnetic axis, i.e. 2.96m (Figure 3). The size of the emitting volume was found by adjusting r_{min} to match the total neutron rates projected from the TOFOR flux with the total rates measured by the JET fission chambers, R_{NT},

$$\frac{I_{LOS}}{\Omega_{LOS} V_{LOS}} V_{TOT} = R_{NT} \quad (1)$$

where V_{TOT} is the total size of the emitting plasma volume given by $2\pi^2 \cdot R_{maj} \cdot r_{min}$.

The measured TOFOR t_{TOF} spectrum is analyzed with a Bayesian forward fitting routine. The neutron energy spectrum is divided into components describing different physical processes in the plasma. These are subsequently folded with the TOFOR response function and fitted to the measured t_{TOF} data using the method suggested by Cash [15].What components are used in the fit depends on the experiment scenario. The components are parameterized and the parameters varied in the fit. As an example, the thermonuclear emission is represented as a Gaussian defined by its intensity and its width $\sigma = 37.5T_d^{1/2}$. The TOFOR response function is created through GEANT4 [16] simulations of quasi-monoenergetic neutrons in 50keV intervals from 1-11MeV. It is normalized to give the response per neutron, which means that the intensity results from the fit correspond to the number of neutrons of a certain energy incident on the primary TOFOR detector. In the analysis, neutrons emitted directly into the TOFOR line-of-sight as well as energy-degraded neutrons that scatter off tokamak structures before reaching TOFOR need to be taken into account [17]. The level of scattered neutrons is proportional to the total neutron yield from the plasma. In the analysis of spectra with low statistics such as the ones studied here, the intensity of the scattered component is fixed to a fraction of R_{NT} (determined from fitting to TOFOR data from high intensity JET pulses).

3. SIMULATIONS

The Monte Carlo code ControlRoom [18] has been used to investigate the energy spectrum of reaction products as well as absolute reaction rates of the $^9Be(^3He,n)^{11}C$, $d(^3He,p)\,\alpha$, $^9Be(\alpha,n)^{12}C$ and $^9Be(p,n)^9B$ reactions. ControlRoom calculates reactivities and emitted particle energy spectra based on given ion densities and velocity. The code samples the velocity distributions of the two reacting particle species, including cyclotron motion and pitch angle; the velocity distributions can be of arbitrary shape. From the sampled velocities, the energies of the reaction products are calculated. In the simulations presented in this paper, a population of 10^6 samples where used to obtain a statistical description of the energy spectrum of the reaction products. An earlier version of ControlRoom (Apache, main upgrade between the two was a change of programming language from C to C^{++}) was used in ref 6 to predict the α knock-on tail the observation of which was later reported in [7].

The energy of the neutrons emitted in the reactions $^9Be(^3He,n)^{11}C$, $^9Be(\alpha,n)^{12}C$ and $^9Be(p,n)^9B$ depends on the energies of the reactants, the reaction Q-value (Q = 7.6MeV, Q = 5.7MeV and Q = –1.9MeV, respectively) and the excitation energies of the resulting carbon nuclei. For detection with TOFOR, E_n>1MeV is required. Thus, for $^9Be(^3He,n)^{11}C$, neutrons produced in conjunction with ^{11}C in the ground state or any of the five excited states at 2.0, 4.3, 4.8, 6.3 and 6.5MeV can be observed. ^{12}C from $^9Be(\alpha,n)^{12}C$ has one excited state at 4.44MeV that, in addition to the ground state, can lead to an observable neutron. A major source of uncertainty in simulations of this kind is the cross section information available. Reliable cross section data for the ground state and first excited state of the $^9Be(\alpha,n)^{12}C$ reaction were found [19] and used in the simulation (Figure 4).

Data from [20, 21, 22] on $^{9}Be(p,n)^{9}B$ were combined to cover the whole energy range needed (Figure 4). Experimental results for the total cross section of $^{9}Be(^{3}He,n)^{11}C$ are presented in [23, 24, 25]. These results are used in the simulations, with an extrapolation to energies below $E_{^3He}$ = 1.95MeV as visualized in Figure 4. The shape of the curve below $E_{^3He}$ = 1.95MeV follows that of ground- and first excited state measurements in [26]. Differential cross section measurements were found from $E_{^3He}$ = 596keV upwards [27]; the measurements were used to project the total cross section level at this energy.

Only fragmentary data on the cross sections for the different excited states of the ^{11}C nucleus have been found. Total cross section data are only available for the ground state and first excited state [26]. Differential cross section data at 0 degree lab angle are found in [28] for the ground state and first five excited states, but these are not in agreement with the results from [26]. As a minimum-bias assumption, we decided to base the simulations for $^{9}Be(^{3}He,n)^{11}C$ on the assumption of equal branching ratios for the ground state and the first four excited states. Two different uncertainties are introduced in this way. Firstly, setting the branching ratios for higher excited states not observable with TOFOR to zero leads to an uncertainty in the absolute contribution from $^{9}Be(^{3}He,n)^{11}C$ neutrons to the total neutron yield rate. Secondly, assuming equal branching ratios for the excited states in the observable region introduces an uncertainty in the shape of the neutron spectrum.

Neutron spectra from the $^{9}Be(^{3}He,n)^{11}C$, $^{9}Be(\alpha,n)^{12}C$ and $^{9}Be(p,n)^{9}B$ reactions were simulated using $n_e = 2.6\times10^{19}$ m^{-3}, $n_{Be} = 0.01ne$, $n_{^3He} = 0.01n_e$, $n_d = 0.5n_e$, T_{bulk} = 5keV and a Maxwellian 3He distribution. While ^{3}He was seeded to the plasma in this experiment, the main proton and alpha source was the $d(^{3}He,p)\alpha$ fusion reaction (with E_α = 3.6MeV and E_p = 14.7MeV from cold reactions). The $d(^{3}He,p)\alpha$ proton and alpha source terms and their resulting steady-state slowing down distributions were simulated and the results used in the $^{9}Be(\alpha,n)^{12}C$ and $^{9}Be(p,n)^{9}B$ simulations. The α distribution result is shown in Figure 5; the result is similar for p, but with the energy scale modified due to the different birth energy. Note that the shape of the alpha source term is broadened due to the high energy of the ^{3}He reactant (in this example, $T_{^3He}$ = 300keV).

Resulting neutron energy spectra are shown in Figure 6. $T_{^3He}$ = 300 keV was used to produce the results in the figure, but the calculation is easily redone for any value of $T_{^3He}$. As can be seen, these simulations predict the neutron emission rate to be significantly lower for the $^{9}Be(\alpha,n)^{12}C$ and $^{9}Be(p,n)^{9}B$ reactions (panels b and c) than for $^{9}Be(^{3}He,n)^{11}C$ reaction (panel a).

A further simulation was made to investigate to what extent the emission from these reactions could contribute to the neutron emission from the plasma. Using ControlRoom, the reactivities of the fusion reactions $d(d,n)^{3}He$, $^{9}Be(^{3}He,n)^{11}C$ and $d(^{3}He,p)\alpha$ were calculated as functions of temperature. The result for $d(^{3}He,p)\alpha$ was used to determine the $^{9}Be(\alpha,n)^{12}C$ and $^{9}Be(p,n)^{9}B$ neutron emissions as described above. The temperature of the bulk deuterium was varied between 1 and 7keV in the $d(d,n)^{3}He$ simulation, but set to 5keV for the $d(^{3}He,p)\alpha$ simulation. The temperature of the high-energy ^{3}He was varied between 100 and 700keV. The resulting total neutron rates are plotted in Figure 7. Also shown in Figure 7 is the emissivity in the solid angle viewed by TOFOR

(scale to right). If this number is multiplied by the emitting volume in the sight line, V_{LOS}, the neutron rate in the direction of TOFOR is obtained.

There are a few things of particular interest here. First, in a plasma containing a minority of ^{3}He where the protons and alpha particles are produced from d(^{3}He,p)α fusion as in this case, the ^{9}Be(^{3}He,n)^{11}C emission (a single step process) will always dominate over the ^{9}Be(p,n)^{9}B and ^{9}Be(α,n)^{12}C emissions (two step processes) by more than an order of magnitude. At $T_{^3He}$ = 300keV, the summed emission from the two-step reactions will amount to less than 4% of that from ^{9}Be(^{3}He,n)^{11}C . It should be noted that this number is assuming perfect confinement; in fact, losses are expected, especially for the 14.7MeV protons from d(^{3}He,p)α. Since the emission spectrum from the three reactions cover the same energy range (Figure 6), the spectral shape of ^{9}Be(^{3}He,n)^{12}C neutrons will dominate the spectrum. Second, the ratio of d(d,n)^{3}He and ^{9}Be(^{3}He,n)^{11}C emissions will vary with the deuterium and ^{3}He temperatures. For example, assuming a ^{3}He temperature of around 200keV, the emissivities of d(d,n)^{3}He and ^{9}Be(^{3}He,n)^{11}C will be roughly equal in the case of cold JET plasmas with little or no bulk ion heating ($T_{bulk} \approx$ 2keV), while for elevated bulk temperatures (around 5keV), the d(d,n)^{3}He emission will dominate by more than a factor 10. This however poses no principal problems for detecting the ^{3}He induced neutron emission since it is mainly found at neutron energies $E_n >$ 3MeV, where no d(d,n)^{3}He neutrons are expected.

4. EXPERIMENTAL RESULTS

Figure 8 shows summed TOFOR t_{TOF} spectra for (a) ohmic parts of pulses in the interval 73100-73700 and (b) all pulses from the two sessions studied here (Table 1), integrated during the relevant plasma period only. A common feature in the two spectra is the characteristic bulk d(d,n)^{3}He neutron peak at 65ns, broadened in the region 60-70ns, with a continuum towards higher t_{TOF} (70-100ns) as well as a small tail on the low t_{TOF} side of the peak (most clearly visible in the Ohmic data in panel a), attributed to multi- and backscattered neutrons. Also distinguishable in both data sets is a small peak at 27 ns from t(d,n)α reaction neutrons (TBN), at about 1/100 of the 65ns peak amplitude. This peak is expected to show similar features as the main d(d,n)^{3}He peak with scatter towards higher t_{TOF} on a level correspondingly lower than the peak intensity, i.e., below the observable level in the two data sets shown.

In panel b, a significant number of high-energy neutron events (low t_{TOF}) is seen in the region 30-60ns that is not present in the ohmic case. A random contribution to the spectrum of 1.9 events per 0.4ns t_{TOF} bin is subtracted from the data in Figure 8b; this level is much lower than the events seen and fluctuations in the random background cannot explain the data.

4.1 SPECTRAL ANALYSIS

The measured t_{TOF} spectra from all pulses are analyzed with the forward fitting procedure described in section 2. Thermal (see section 2), knock-on, ^{9}Be(^{3}He,n)^{11}C and scattered neutron components are fitted to the data. Contributions from ^{9}Be(p,n)^{9}B and ^{9}Be(α,n)^{12}C, expected to be on a few

percent level of the $^{9}Be(^{3}He,n)^{11}C$ contribution, are neglected in the fit to reduce the degrees of freedom. The shapes of the knock-on and $^{9}Be(^{3}He,n)^{11}C$ neutron components are simulated using ControlRoom with a Maxwellian ^{3}He minority distribution with $T_{^3He} = 300keV$ (based on gamma spectroscopy measurements, see section 2) and a bulk temperature $T_d = 5keV$; their intensities are left as free parameters in the fit. The random event background is treated as a flat level as described in section 2. The intensity of the scattered component is fixed to a fraction of the total neutron yield as measured by the JET fission chambers. An example of a result is shown in Figure 9, where the summed t_{TOF} spectrum for Pulse No's: 73761 and 73762 with similar plasma parameters is shown in panel (a) and the neutron energy representation of the fitted components in panel (b).

In this case, the thermal component is small and cannot be reliably fitted. This turned out to be the case for all pulses with $T_d < 4keV$ in this experimental scenario. Therefore, as a first step in the analysis, a fit in the region 60-70ns was used to determine the bulk deuterium temperature for the pulses with better statistics in the 65ns region (example in Figure 10). For the pulses with lower statistics, the scaling of the $d(d,n)^{3}He$ reactivity with T_d was then used; T_d was determined by comparing the measured thermonuclear $d(d,n)^{3}He$ neutron rate with that from a similar pulse with higher temperature.

The resulting deuterium temperatures and the spectral intensities of the thermal, knock-on and $^{9}Be(^{3}He,n)^{11}C$ components for individual pulses in units of estimated number of neutrons incident on the primary TOFOR detector are listed in Table 2 for all pulses studied. All fits are good as measured by the Cash statistics goodness of fit parameter, with reduced values in the range 0.5-1 (if the solution is correct, the expectation value is 1 [15], similar to reduced χ^2). The last column in Table 2 gives the contribution from $^{9}Be(^{3}He,n)^{11}C$ to the spectrum as a fraction of the total neutron flux. The $^{9}Be(^{3}He,n)^{11}C$ contribution varies in the range from 18 to 30 percent during the first session and from 22 to 64 percent during the second session. This contribution cannot be separated from the $d(d,n)^{3}He$ neutron yield by standard neutron rate diagnostics such as the fission chambers used at JET.

A few observations can be made about the results. The intensity of the thermal component (Table 2) is low in the discharges with low ^{3}He concentration (Table 1). In the second session it peaks for JET Pulse No: 73768, with almost 7 percent ^{3}He. With more ^{3}He, more energy will be transferred to the bulk of the plasma. For Pulse No: 73766, significantly lower neutron rates (too low to perform an analysis) were observed; thesis in line with expectations since the RF resonance layer in this case was moved out of the TOFOR line-of-sight on the low field side ($R_\omega = 3.24m$), by lowering the frequency to $\omega_{RF} = 33MHz$.

4.2 BERYLLIUM CONCENTRATIONS

During session 2, a distinct change in tail shape was observed between early and late pulses from flat in the first few discharges to more concentrated in the high t_{TOF} region in the later pulses, as exemplified by the data for Pulse No's: 73761 and 73768 in Figure 11 a and b, respectively. This

could be attributed to a decrease in beryllium concentration in the vessel during the session; as the ^{9}Be concentration goes down, the high-energy neutron emission will be more dominated by knock-on, falling in the region $t_{TOF} > 50$ns, while for higher ^{9}Be concentrations, neutrons from $^{9}Be(^{3}He,n)^{11}C$ with $E_n < 10$MeV and $t_{TOF} > 35$ns will dominate.

Since the rate of $^{9}Be(^{3}He,n)^{11}C$ reactions is directly proportional to the ^{3}He and ^{9}Be concentrations, a comparison between the measured $^{9}Be(^{3}He,n)^{11}C$ neutron rates (I_{Be}) in Table 2 and the simulated rates per unit volume (Γ_{Be}) in Figure 7 can be used to estimate the beryllium concentration. The simulations are made assuming X [^{3}He] = X [^{9}Be] = 1%, which means the beryllium concentration estimate can be obtained by direct scaling using

$$X[^{9}Be] = \frac{I_{^{9}Be}}{X[^{3}He]\ {}_{^{9}Be}V_{LOS}} \qquad (2)$$

where X[^{3}He] is the measured ^{3}He concentration (Table 1).

The plasma volume viewed by TOFOR, V_{LOS}, is determined using equation (1); a best value r_{min} = 0.375m is deduced by comparing R_{NT} and I_{TOT} for all pulses studied (mean of right side over left side of equation (1) for all pulses is 1.01, with $\sigma = 0.10$). This corresponds to a total emitting volume of 8.2m^3. The estimate is confirmed by the tomographic reconstruction of the measured gamma emission profile [29] for Pulse No: 73205 (Figure 12); 8.2m^3 cover 93% of the tomogram intensity.

$T_{^{3}He}$ = 300 keV (estimated uncertainty ±20%) is again assumed in the analysis based on the gamma spectroscopy results in section 2. Resulting estimated beryllium concentrations are plotted in Figure 13. A clearly decreasing trend is seen for session 2 which explains the observation in Figure 11. Pulse No's: 73766, 73213 and 73214 with RF resonance layers outside of the TOFOR line of sight are excluded in the analysis.

5. DISCUSSION

The plasma scenario studied here, with cold bulk deuterium plasma, beryllium evaporation and ICRH tuned to minority ^{3}He is unusual by today's standards. However, beryllium will be an important impurity at ITER, and also at JET after the upcoming installation of the ITER like wall, and beryllium reactions will need to be taken into account. The rate of $^{9}Be(^{3}He,n)^{11}C$ reactions in hydrogen plasmas with ICRF heating on ^{3}He minority could limit the feasibility of this scheme during the ITER low-activation phase. A quick estimate using the ControlRoom simulation described in section 3, assuming X [^{3}He] = X [^{9}Be] = 2%, a Maxwellian ^{3}He distribution with $T_{^{3}He}$ = 150keV, a 60m^3 emitting plasma volume and a pulse duration of 1500s gives a neutron emission per pulse of the order 10^{18}; this is comparable to the t(d,n)α neutron emission in the JET record fusion power Pulse No: 42976 (5×10^{18}).

The impact on the surrounding structures from neutrons in the range 1-10MeV will be quite different from that from the same amount of neutrons in the energy range 2-3MeV. The substantial contribution to the neutron spectrum from non- $d(d,n)^{3}He$ neutrons also has to be considered when

measured neutron rates are used to provide estimates of achieved fusion power, and when they are benchmarked against simulation codes such as TRANSP.

5.1 IMPURITY REACTIONS

The neutron spectrum measured in these experiments has been shown to be consistent with the expected neutron emission from the reaction $^{9}Be(^{3}He,n)^{11}C$. However, neutrons from other impurity reactions will also be present; $^{9}Be(\alpha,n)^{12}C$ and $^{9}Be(p,n)^{9}B$ contribute on a few percent level. With a different plasma scenario, other reactions will become more important. At JET, experiments with bulk ^{4}He plasmas are planned; in this case, substantial amounts of $^{9}Be(\alpha,n)^{12}C$ neutrons will be produced. With RF heating on fundamental hydrogen, $^{9}Be(p,n)^{9}B$ may become significant and need to be taken into account.

The effect of the fast ion distribution on the resulting neutron spectrum can be significant. In section 3, $^{9}Be(\alpha,n)^{12}C$ and $^{9}Be(p,n)^{9}B$ neutron spectra were simulated for fusion-born alpha and protons from $d(^{3}He,p)\alpha$ (Figure 6). If instead Maxwellian distributions with T = 300keV are used, the result will be as in Figure 14 (with $n_e = 2.6\times10^{19}$ m^{-3}, $n_{Be} = 0.01n_e$, $n_{^4He} = 0.01n_e$ and $n_p = 0.01n_e$).

The neutrons seen in [10] as discussed in the introduction do not match the spectral shape of the $^{9}Be(p,n)^{9}B$ reaction as simulated here; however, the shape closely follows that expected from deuterium heated with 2^{nd} harmonic ICRF (see e.g. [14]), competing with fundamental hydrogen heating at the same resonance position.

5.2 BULK DEUTERIUM TEMPERATURES

The established strength of neutron emission spectroscopy is the ability to provide bulk fuel ion temperatures. In the case of the peculiar plasma scenario studied here, the bulk deuterium temperature can be reliably derived if the fit is performed in the region of the spectrum around 2.5MeV where thermonuclear $d(d,n)^{3}He$ events dominate. The simulated rates (Figure 7) at the temperatures derived from the fit to the data have been checked against the measured rates as a cross-benchmark of both simulations and analysis, using the ratio $\Gamma_{thermal}(T_d)*V_{LOS}/I_{thermal}$. With perfect agreement between measurements and simulations, this ratio should be 1; the mean for all pulses is 1.56, with $\sigma = 0.61$. This is well within the limits of the involved uncertainties (e.g., ±1keV in derived T_d, and 30% on Z_{eff} used to obtain n_d from n_e).

5.3 BERYLLIUM CONCENTRATIONS

The nice agreement between simulations and analysis obtained for the thermal component strengthens the argument of using equation (2) to determine the beryllium concentration. Some observations can be made about Figure 13. Firstly, the concentration is expected to be higher for the second session than for the first due to the amount of evaporation, with four heads in the second session compared to two in the first; this is indeed observed. Secondly, the time evolution of the deduced beryllium concentration is in agreement with measurements on visible bremsstrahlung, represented

by the solid red curve in the figure. The measurement is for X[Be]/X[C] and it has been normalized to the TOFOR beryllium concentration value for Pulse No: 73761. If the level of carbon impurities is assumed to be constant for the pulses studied, the time evolution of X[Be]/X[C] is expected to agree with the values from the analysis presented here.

Thirdly, the peak value X[^{9}Be] = 5% observed at the beginning of the second session is rather high. There are many factors affecting the uncertainty in the absolute level. The estimated statistical uncertainties have been incorporated in the plotted error bars of about ±40%; they come from uncertainties in ^{3}He reactivity (29%), the emitting plasma volume (10%), the fit to TOFOR data (11-21%), $n_{^3He}$ (20%) and n_e (10%). The dominating contribution to the statistical uncertainty is the ^{3}He reactivity. The assumed uncertainty in the $T_{^3He}$ = 300keV used is then 20%. The assumption of a Maxwellian distribution also introduces an uncertainty in the reactivity of the ^{3}He population.

Systematic uncertainties are not included in the error bars. The most important systematic uncertainty comes from the assumptions on the cross sections of the different excited states of carbon populated in the ^{9}Be(^{3}He,n)^{11}C reaction as described in section 3. Excluding the higher excited states introduces an uncertainty in the absolute level of the deduced beryllium concentrations. The assumption of equal branching ratios to the lower excited states also affects the analysis; if the statistics of the TOFOR data were higher, the validity of this assumption could be tested by fitting individual peaks to the data. As it is, suffice it to observe that an uncertainty is introduced. This uncertainty could have an impact on the fitted intensity of the knock-on component. The knock-on intensity is lower than expected; if a lower cross section was assumed for the carbon states in the region of the knock-on component, the fitted intensity of this component would increase. Also neglecting ^{9}Be(α,n)^{12}C and ^{9}Be(p,n)^{9}B reactions will affect the absolute level; if 5% of the neutrons now attributed to ^{9}Be(^{3}He,n)^{11}C reactions could instead be ascribed to these two, then the estimated Be concentration would exhibit a corresponding 5% drop.

CONCLUSIONS

The main result presented in this paper is the observation of a substantial contribution, in the range 18-64 percent, to the neutron emission spectrum from deuterium plasmas from ^{9}Be(^{3}He,n)^{11}C reactions. This reaction is established as the origin of the observed neutrons by comparing Monte Carlo simulated neutron energy spectra with TOFOR data. Simulated and measured spectral shapes are seen to be consistent. ^{9}Be(α,n)^{12}C and ^{9}Be(p,n)^{9}B reactions are also simulated and ^{9}Be(^{3}He,n)^{11}C is shown to dominate over ^{9}Be(α,n)^{12}C and ^{9}Be(p,n)^{9}B for the plasma scenario studied.

TOFOR's main use is as a fast ion diagnostic for study of the deuterium distribution. In spite of the low counting statistics in the experiment analyzed in this paper, excellent agreement is seen between simulations and TOFOR measurements for the bulk deuterium distribution. The knock on component also provides evidence of the build-up of a fast deuterium population. Through the observations of ^{9}Be(^{3}He,n)^{11}C neutrons (and (^{3}He)D knock-on), clear evidence is provided of the presence also of ^{3}He tails. We show that TOFOR can be used to estimate the beryllium concentration

in the plasma. The time evolution of the beryllium concentration derived from TOFOR data is consistent with that from visible bremsstrahlung measurements.

The $^{9}Be(^{3}He,n)^{11}C$, $^{9}Be(\alpha,n)^{12}C$ and $^{9}Be(p,n)^{9}B$ neutron spectra cover the range 0-10MeV, while the neutron emission from a regular NB heated deuterium plasma falls mainly in the interval 2-3MeV. The regions overlap and a neutron spectrometer such as TOFOR is an essential tool for separating the anomalous neutrons from the ones from ordinary $d(d,n)^{3}He$ fusion reactions.

The importance of reactions involving beryllium impurities will increase with the introduction of beryllium-coated vessel walls at JET and at ITER. We estimate that the integrated neutron emission from $^{9}Be(^{3}He,n)^{11}C$ reactions from one ITER hydrogen plasma pulse during the low activation phase could be 10^{18}.

TOFOR can be used together with gamma diagnostics and the NPA to study fast ions not only in deuterium plasmas but also in hydrogen, ^{3}He and ^{4}He plasmas, where neutrons from $^{9}Be(p,n)^{9}B$, $^{9}Be(^{3}He,n)^{11}C$ and $^{9}Be(\alpha,n)^{12}C$ reactions will dominate.

ACKNOWLEDGEMENTS

We acknowledge the contribution of S.Popovichev, who helped with the running of the TOFOR spectrometer at JET.

REFERENCES

[1]. Gormezano C et al 2007 *Nuclear Fusion* **47** S285-S336

[2]. Van Ester D, Louche F and Koch R 2002 *Nuclear Fusion* **42** 310-328

[3]. Pinches S.D. *et al* 2006 *Nucl. Fusion* **46** S904-S910

[4]. Sharapov S.E. *et al* 2005 *Nuclear Fusion* **45** 1168-1177

[5]. Brysk H 1973 *Plasma Physics* **15** 611-617

[6]. Ballabio L, Gorini G and Källne J 1997 *Physical Review* E **55** 3358-3368

[7]. Källne J, Ballabio L, Frenje J, Conroy S, Ericsson G, Tardocchi M, Tranéus E and Gorini G 2000 *Physical Review Letters* **85** 1246-1249

[8]. Nocente M *et al* Simulation of neutron emission spectra for RF heated (3He)D plasmas *to be published*

[9]. Ballabio L, Frenje J, Källne J, Conroy S.W, Ericsson G, Tardocchi M, Traneus E and Gorini G 2000 Nuclear Fusion **40** 21-33

[10]. Jarvis O.N. 1994 *Plasma Physics and Controlled Fusion* **36** 209-244

[11]. Mantsinen M.J, Jarvis O.N, Kiptily V.G, Sharapov S.E, Alper B, Eriksson L.G, Gondhalekar A, Heeter R.F. and McDonald D.C. 2001 *Nuclear Fusion* **41** 1815-1822

[12]. Kiptily V.G, Popovichev S, Sharapov S.E, Bertalot L, Cecil F E, Conroy S and Mantsinen M J 2003 *Rev. Sci. Inst.* **74** 1753-1756

[13]. Mayoral M-L *et al.* 2006 *Nuclear Fusion* **46** S550–S563

[14]. Gatu Johnson M et al 2008 *Nuclear Instruments and Methods in Physics Research* A **591** 417 430

[15]. Cash W. 1979 *Astrophys J* **228** 939-947
[16]. Agostinelli S *et al* 2003 *Nucl Inst Meth A* **506** 250-303
[17]. Gatu Johnson M *et al* 2008 *Burning Plasma Diagnostics An International Conf. Varenna Italy 24-28 September 2007* Orsitto F P, Gorini G, Sindoni E and Tardocchi M Melville New York AIP Conf. Proc 988 311-314
[18]. Ballabio L *Calculation and Measurement of the Neutron Emission Spectrum due to Thermonuclear and Higher-Order Reactions in Tokamak Plasmas PhD Thesis, Acta Universitatis Upsaliensis No. 797* 2003 Faculty of Science and Technology Uppsala University
[19]. Kiptily V.G. *et al.* 2002 *Nuclear Fusion* **42** 999-1007
[20]. Marion J.B. 1956 *Physical Review* **103** 713-717
[21]. Walker B.D, Wong C, Anderson J D and McClure J W 1965 *Physical Review* **137** B1504-B1508
[22]. Byrd R.C, Floyd C.E, Guss P.P, Murphy K and Walter R L 1983 *Nuclear Physics* **A399** 94-118
[23]. Guzhovskij B JA, Abramovich S N and Pereshivkin V A *Measurement of C-11 radionuclide formation total cross sections in B-10(D,N)C-11, BE-9(HE3,N)C-11, B-11(D,2N)C-11 reactions by activation method* REF (J,YK,,(2),55,84) (from EXFOR)
[24]. Hahn R.L and Ricci E 1966 *Phys. Rev.* **146** 650-659
[25]. Anders B, Herges P and Scobel W 1981 *Z. Phys.* A **301** 353-361
[26]. Din G.U and Weil J.L 1965 *Nucl. Phys.* **71** 641-661
[27]. Serov V.I and Guzhovskij B.J 1962 *Atomnaya Energiya* **12** 5
[28]. Duggan J.L, Miller P.D and Gabbard R F 1963 *Nucl. Phys.* **46** 336-352
[29]. Kiptily V.G *et al.* 2005 *Nuclear Fusion* **45** L21-L25

Session	JET Pulse No:	I_P [MA]	P_{RF} [MW]	X[^{3}He] [%]
1	73204	2.2	5.0/3.0	≈5
	73205	2.5	5.4	≈4
	73207	2.5	3.5	3.3
	73210	2.5	3.5	3.8
	73212	2.5	5.2/4.0	3.7
	73213	2.5	3.0	3.7
	73214	2.5	5.0/3.2/2.0	3.7
	73216	2.5	3.4/4.8/3.4/1.0	3.6
	73217	2.5	3.4/5.4	3.6
2	73761	2.5	4.0	1.2
	73762	2.5	4.0	1.2
	73764	1.8	4.7	1.4
	73765	3.0	4.5	1.5
	73766	3.0	3.0	1.6
	73768	2.5	6.0	6.8
	73769	2.2	6.0	3.0

Table 1: Summary of relevant plasma conditions for the pulses studied in this paper: Plasma current I_P, RF power P_{RF} and ^{3}He concentration (average from ^{3}He real-time control).

JET Pulse No:	T_d [keV]	I_{TH} [x10^4]	I_{Be} [x10^4]	I_{KN} [x10^4]	I_{Be}/I_{total}
73204	4.0±1.0	4.2±0.3	1.9±0.4	4.8±2.8	0.30±0.07
73205	6.0±0.9	10±0.6	4.1±0.5	3.0±0.6	0.23±0.04
73207	5.2±1.0	7.5±0.5	2.5±0.4	0.63*	0.24±0.05
73210	5.4±0.9	7.2±0.5	2.5±0.4	0.01*	0.25±0.05
73212	4.2±1.0	7.9±0.5	2.2±0.4	2.5±0.5	0.18±0.04
73213	5.6±1.1	6.2±0.5	2.1±0.4	1.4±0.4	0.21±0.05
73214	4.4±1.0	6.1±0.5	2.2±0.4	1.9±0.5	0.22±0.05
73216	5.1±0.9	6.1±0.4	1.3±0.3	0.01*	0.18±0.05
73217	5.6±1.1	6.9±0.5	2.3±0.4	1.1±0.4	0.22±0.05
73761	3.2±0.4	1.3±0.2	3.1±0.4	0.62±0.03	0.62±0.13
73762	3.7±0.5	1.3±0.2	3.3±0.4	0.49±0.03	0.64±0.14
73764	3.8±0.5	2.0±0.3	2.3±0.4	1.3±0.4	0.41±0.10
73765	5.1±0.8	3.8±0.4	3.5±0.4	1.5±0.5	0.40±0.07
73768	6.3±1.0	6.9±0.5	2.4±0.4	1.4±0.5	0.22±0.05
73769	4.1±0.6	2.6±0.3	2.7±0.4	3.0±0.5	0.32±0.07

*The intensity is too low for a reliable fit; upper limits are given.

Table 2: Bulk deuterium temperatures and intensities (number of neutrons incident on the primary TOFOR detector) derived from fitting a thermal, a ^{9}Be(^{3}He,n)^{11}C, a knock-on and a scatter component to the data from the JET pulses given in the left column. Also shown is the relative contribution from ^{9}Be(^{3}He,n)^{11}C neutrons to the total neutron spectrum (right column).

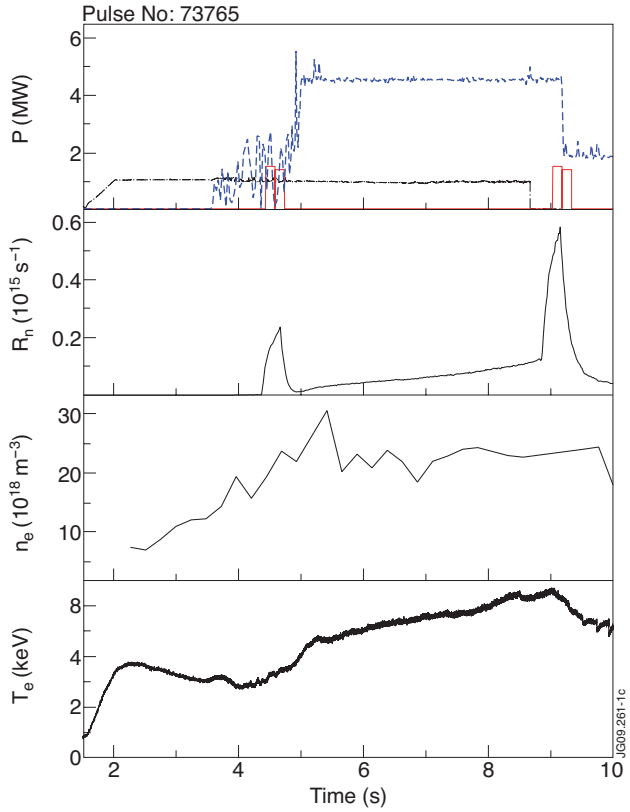

Figure 1: Time-resolved data for JET Pulse No: 73765. The top panel shows the ICRH power (dashed blue), the LHCD power (dotted black) and the NBI power (red), the second panel the neutron yield from the fission chambers, the third the on-axis electron density from LIDAR Thomson scattering and the fourth the electron temperature from heterodyne radiometer measurements.

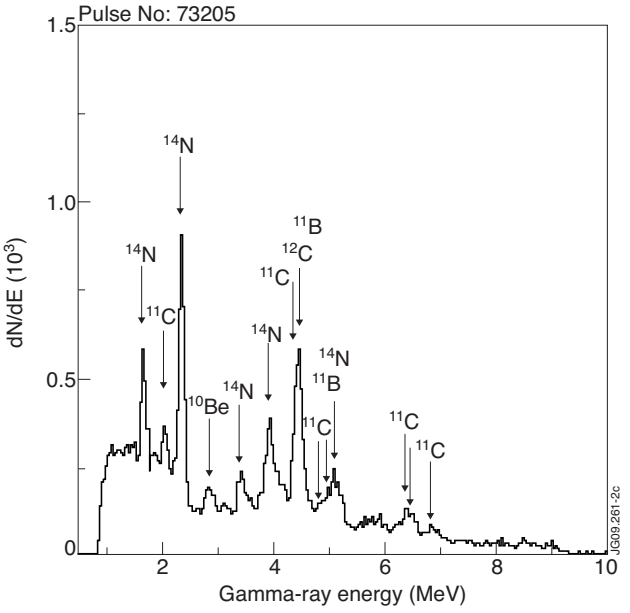

Figure 2: Gamma spectroscopy data for Pulse No: 73205 from a NaI crystal in the TOFOR line of sight about 3.5m further away from the tokamak. Analysis of the ^{14}N, ^{11}C and ^{11}B peaks yields information about fast ^{3}He in the JET vessel.

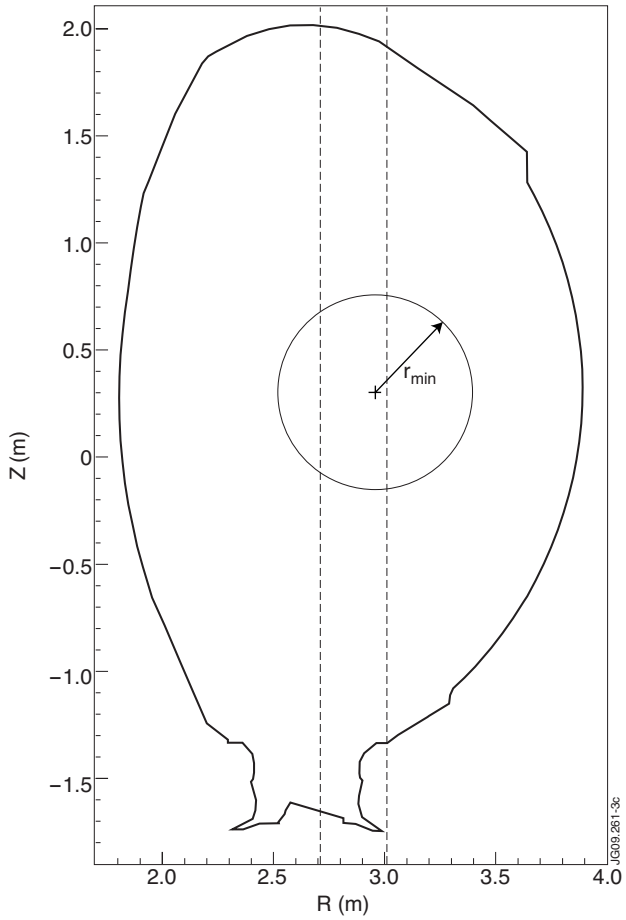

Figure 3: Poloidal cross section of the JET vessel showing the vertical sight line of TOFOR (solid lines). The emitting volume, bounded by r_{min}, used in the analysis of TOFOR data is also illustrated.

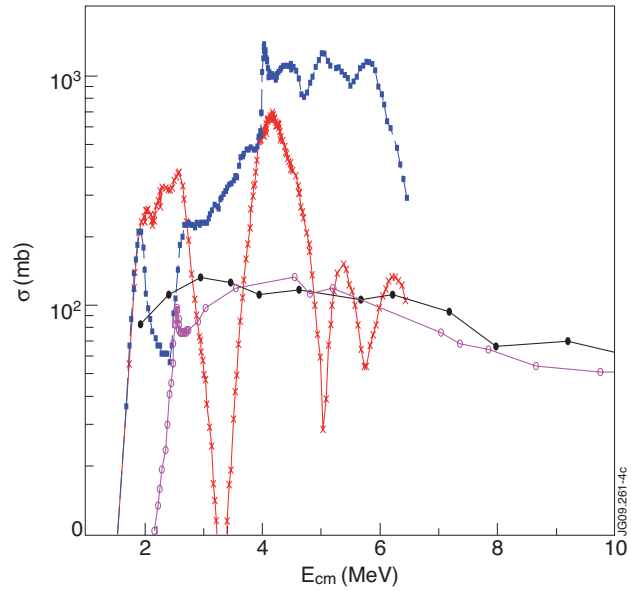

Figure 4: Total cross section for $^{9}Be(^{3}He,n)^{11}C$ (black dotted), $^{9}Be(p,n)^{9}B$ (magenta, hollow circles) and ground state and first excited state cross sections for $^{9}Be(\alpha,n)^{12}C$ (red crosses and blue squares) used in the ControlRoom simulations, as functions of center of mass energy, ECM. The points represent measured data from references [19, 20, 21, 22, 23, 24, 25]; the curves interpolated values used at energies between the measurement points. Note that the $^{9}Be(^{3}He,n)^{11}C$ cross section has been extrapolated down to 1MeV as described in the text.

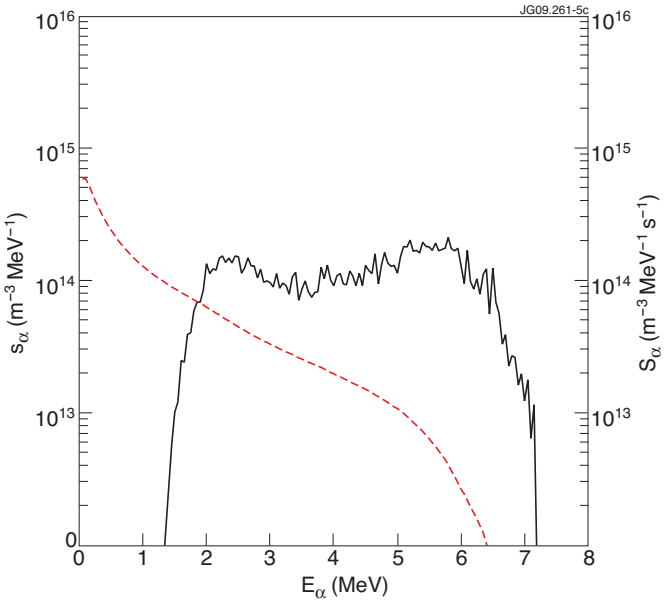

Figure 5: Alpha source term (S_α) from $^3He(d,p)\alpha$ fusion (solid blue) and the corresponding slowing down distribution n_α (dashed red), both shown as functions of alpha particle energy, simulated using Control Room, with assumptions described in the text.

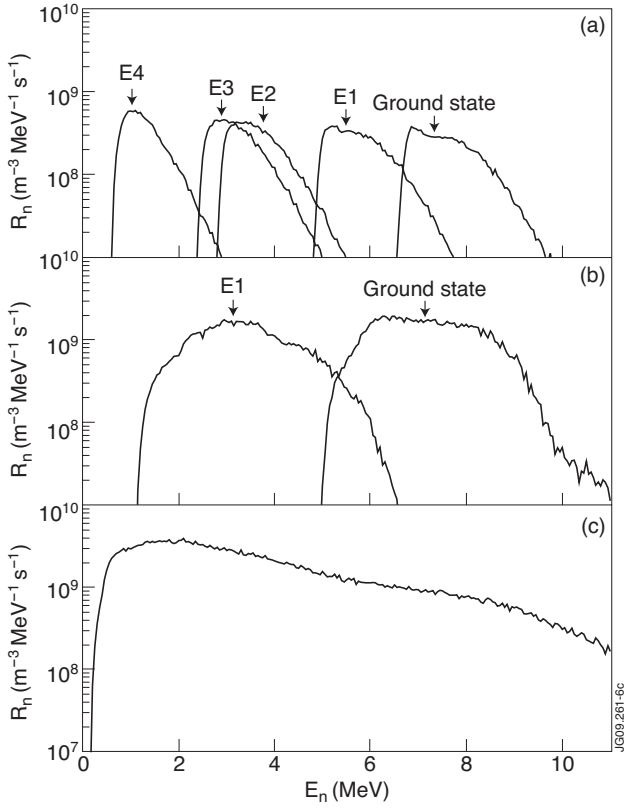

Figure 6: Simulated neutron spectra for (a) $^9Be(^3He,n)^{11}C$, (b) $^9Be(\alpha,n)^{12}C$ and (c) $^9Be(p,n)^9B$, showing the excited states of the carbon nuclei included in the simulations.

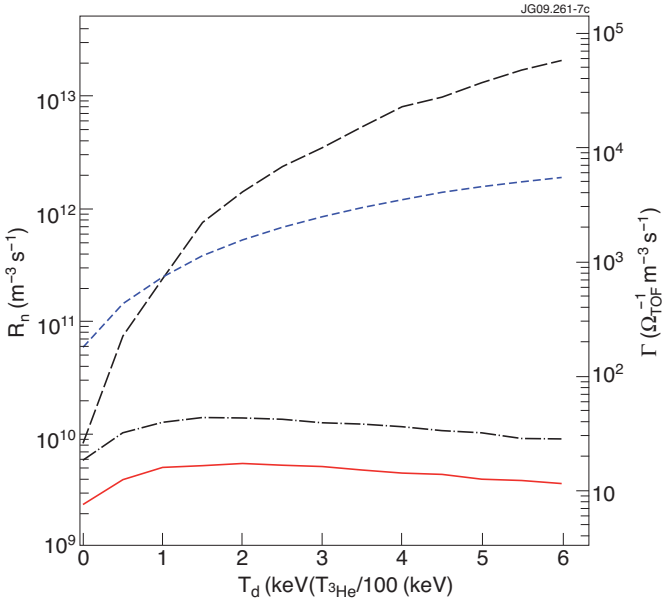

Figure 7: $^9Be(^3He,n)^{11}C$ (short-dash blue), $^9Be(\alpha,n)^{12}C$ (solid red) and $^9Be(p,n)^9B$ (dash-dot black) neutron rates as functions of T_{3He} (Tx100) and $d(d,n)^3He$ (dashed black) neutron rate as a function of bulk deuterium temperature (T_d). The left scale shows the total neutron emission rate per plasma volume for the plasma conditions given in the text, the right hand scale the estimated number of neutrons emitted per unit plasma volume in the solid angle viewed by TOFOR (Ω_{LOS}). Note that the ^3He temperature is shown divided by 100.

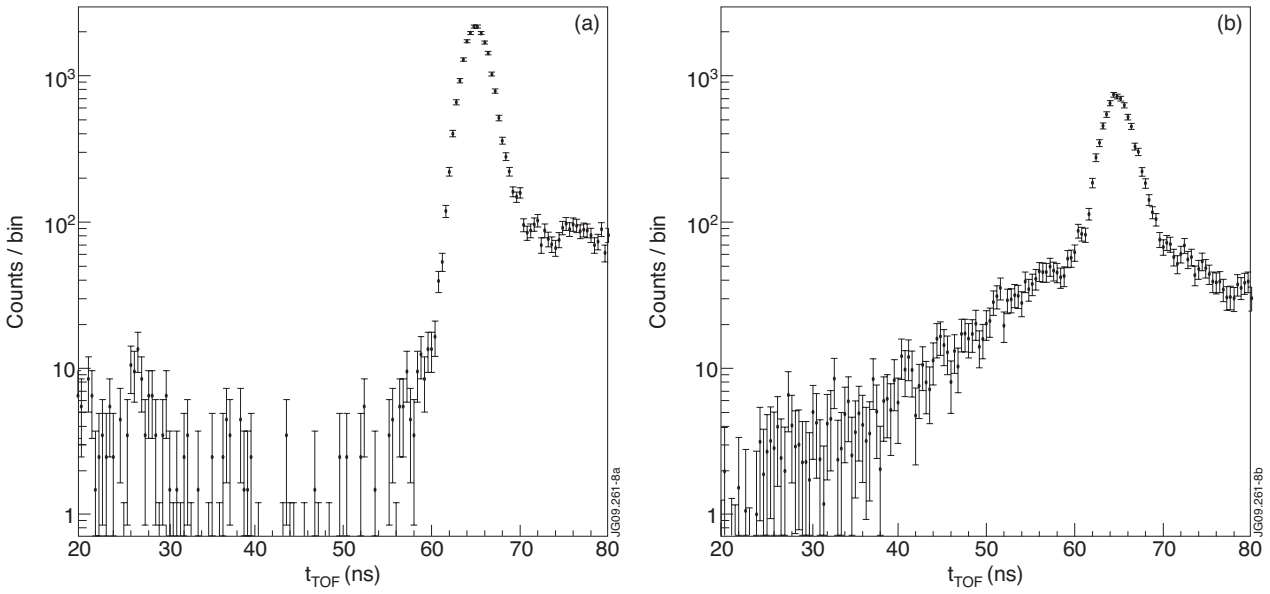

Figure 8: Integrated t_{TOF} spectrum for ohmic parts of pulses in the interval 73100-73700 (panel a) and for the relevant periods of the pulses listed in Table 1 (panel b). A random level based on data on the negative t_{TOF} side has been subtracted in both cases.

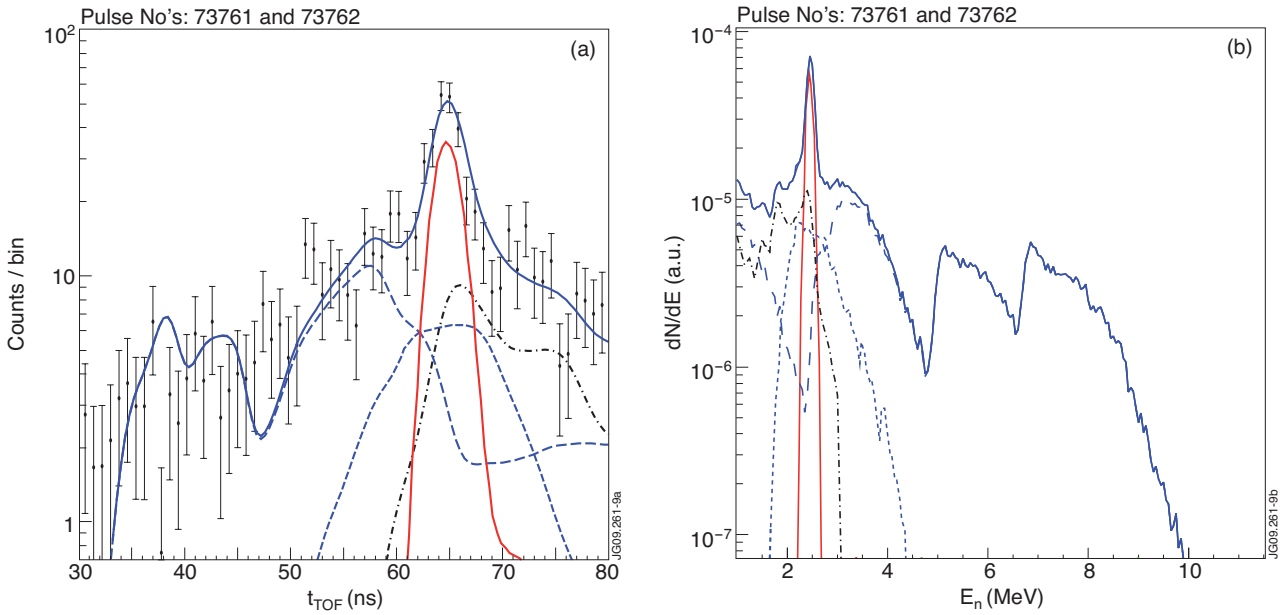

Figure 9: (a) Background subtracted summed TOFOR data for t=5-8.8s from JET Pulse No's: 73761 and 73762, shown with the total best fit to the data (solid blue), thermal (solid red), knock-on (short dash blue), $^{9}Be(^{3}He,n)^{11}C$ (long dash blue) and scattered (dash-dot black) neutron components indicated. (b) Neutron spectrum derived from the component analysis of the data in (a).

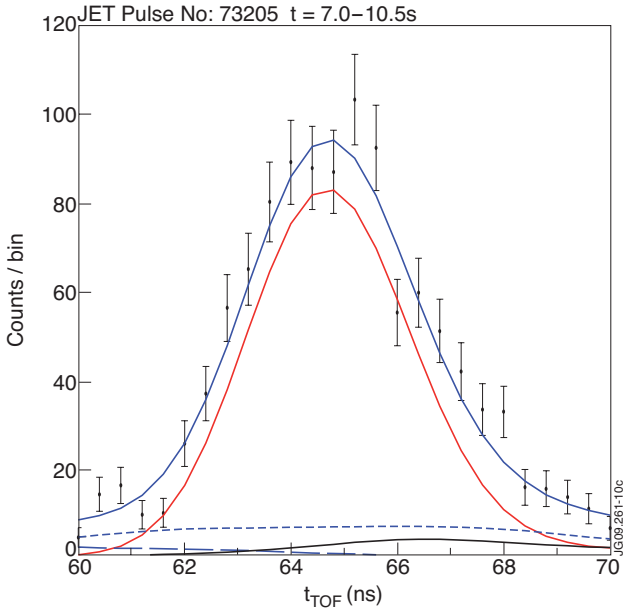

Figure 10: Fit to the peak region of the t_{TOF} spectrum for JET Pulse No: 73205, used to determine the bulk deuterium temperature. The red curve represents the thermal component, blue the summed intensity. The short and long dash blue and the black curves represent the knock-on, $^{9}Be(^{3}He,n)^{11}C$ and scatter components. In this example, $T_d = 6keV$.

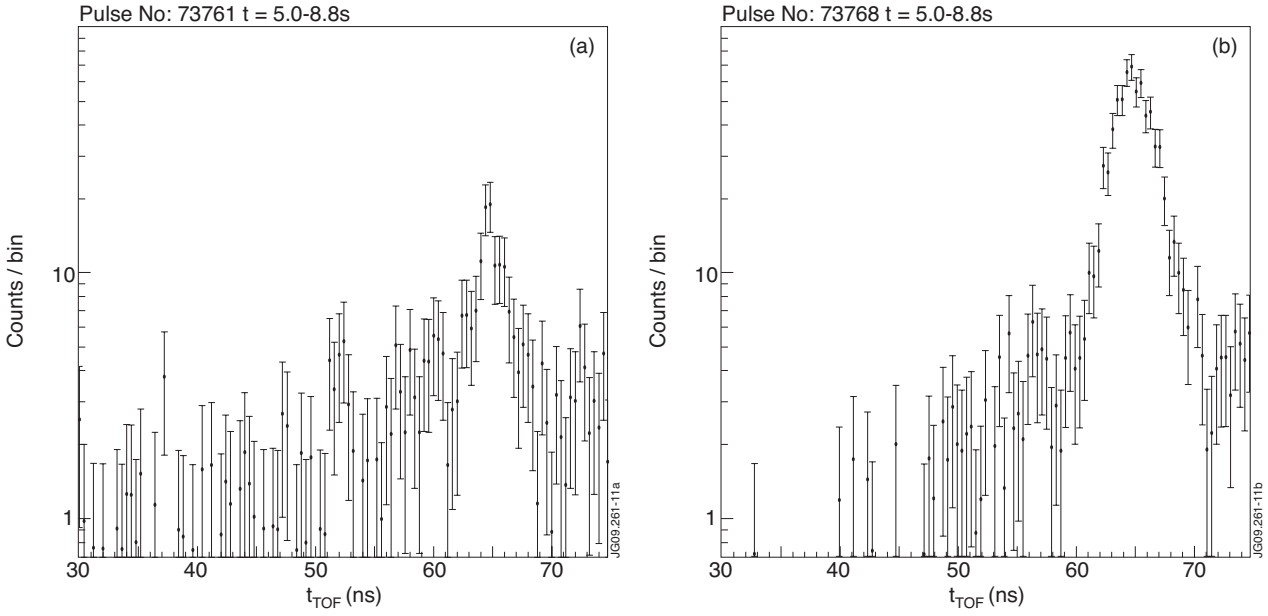

Figure 11: Data for Pulses No's: 73761 (first in session 2, X [^{3}He]~1.2%) and 73768 (late in session 2, X[^{3}He]~6.8%).

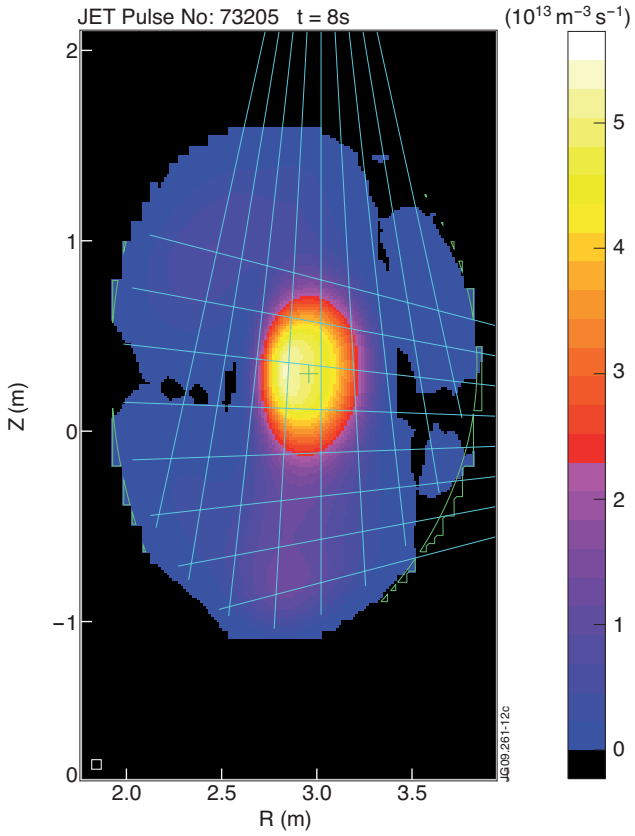

Figure 12: Tomographic reconstruction of the gamma emission profile for Pulse No: 73205 (t = 8-8.5s), as measured by the gamma profile monitor.

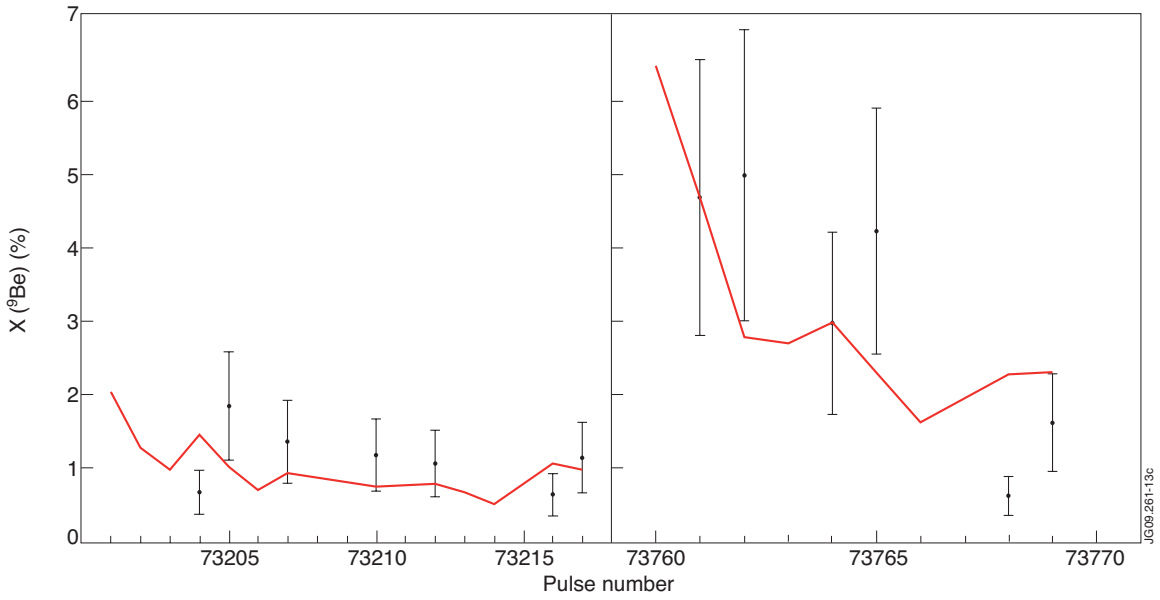

Figure 13: Beryllium concentrations deduced through comparing measured $^{9}Be(^{3}He,n)^{11}C$ neutron rates with simulated rates for (a) session 1 and (b) session 2 (points with error bars). Also shown is the X[Be] / X[C] trend from visible bremsstrahlung measurements, normalized to the TOFOR result for Pulse No: 73761 (red curve).

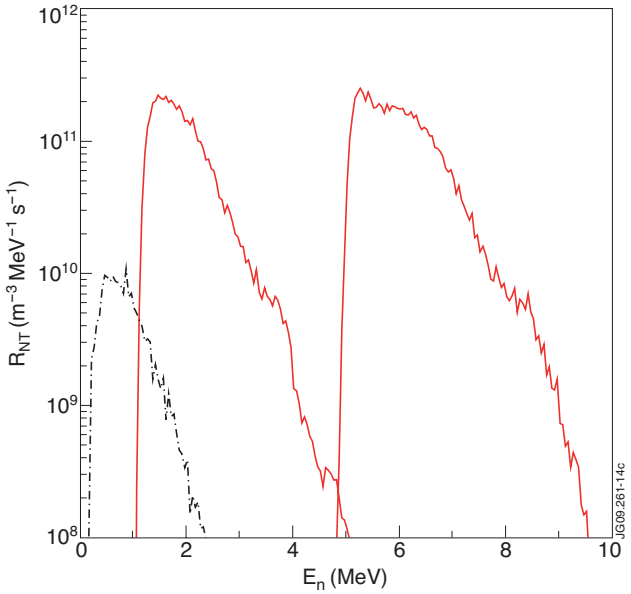

Figure 14: Neutron spectra from $^{9}Be(\alpha,n)^{12}C$ (solid red, ground and first excited states) and $^{9}Be(p,n)^{9}B$ (dash dot black) reactions assuming Maxwellian alpha and proton distributions with T=300keV instead of a $d(^{3}He,p)\alpha$ source term (with impurity levels of $0.01n_e$ and $n_e = 2.6\times10^{19}$ m^{-3}).